World Conference on
Timber Engineering
Oslo 2023

NUMERICAL ANALYSIS OF BIAXIAL HOLLOW TIMBER SLAB ELEMENTS

Dominik Bissig[1], Marcel Muster[2], Andrea Frangi[3]

ABSTRACT: The inventions of the company Timber Structures 3.0 (TS3) facilitate the construction of point supported flat slabs made of cross laminated timber (CLT) elements. The CLT of the entire slab area is designed to bridge the largest span and to resist the largest forces at the point supports. Thus, major portions of the flat slab are overdesigned and much of the built-in structural timber is wasted. To tackle this problem, a biaxial hollow timber slab element is developed, to replace the CLT elements wherever their high performance is not needed. The hollow elements consist of a grid of notched, linear timber beams, covered on both sides with thin CLT plates. The notches in the timber grid cause stress concentrations perpendicular to the grain that can lead to an early brittle failure in regions with large shear forces. Therefore, possibilities to optimise the hollow elements' shear resistance are analysed with the help of finite element (FE) models. The models are compared to experimental results and the chosen methods are validated. The geometry of the FE model is parametrised, and the results of 1024 geometry combinations are analysed to study the influence of the geometry parameters on the structural properties of the hollow elements. The results show that geometries with multiple smaller notches have a significantly higher shear resistance than those with only one notch. Furthermore, the shear resistance can be increased by using a wider web with a smaller spacing. Contrary to the initial assumption, the use of CLT instead of glued laminated timber (GLT) in the web grid does not lead to a significant increase of the shear resistance.

KEYWORDS: TS3, point supported flat slab, biaxial hollow slab elements, FEM, Abaqus, parameter study

1 INTRODUCTION

Point supported flat slabs are often used to build modern office buildings and apartments, allowing for versatile floor plans. Most of these slabs are built with reinforced concrete, a low-cost building material that is well known and widely available. The goal of the company Timber Structures 3.0 (TS3) is to provide a cost efficient and sustainable timber alternative to concrete flat slabs. Thus, TS3 has initiated several research projects to develop a point supported timber flat slab. It consists of cross laminated timber (CLT) elements, which are connected on site with the TS3 resin [1]. The timber flat slab has been realised in several projects in Switzerland [2], but the high strength and stiffness of CLT is not needed in all areas of the point supported slab. Thus, the idea of a biaxial hollow timber slab was presented in [3]. An additional research project was launched in 2021 to investigate the biaxial hollow slab. The goal of the project is to replace the CLT elements in those parts of the slab, where the mass timber solution is not needed from a structural point of view. The conceptual idea of the new hollow slab system is illustrated in Figure 1. The new hollow elements aim to optimise the material usage and to be even more economically competitive than the current TS3 slab system by reducing the amount of valuable structural timber needed. The aim is for the hollow elements to contain at least 30% less timber than CLT elements of an equivalent thickness.

The biaxial hollow slab elements are composed of a bottom and a top CLT plate that are glued to a grid of

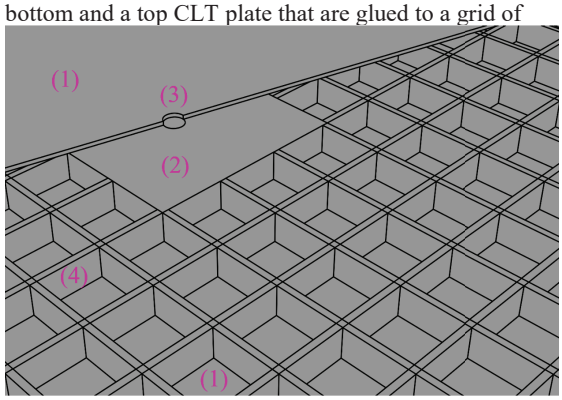

Figure 1: *Sketch of the conceptual idea for a biaxial hollow timber flat slab. (1) upper and lower CLT plate, (2) column head made of CLT, (3) connection and load transfer support, (4) hollow slab grid for biaxial load carrying action.*

linear glued laminated timber (GLT) beams, as illustrated in Figure 1. Figure 2 shows three possibilities how the intersection points of the grid can be accomplished with notches. As presented in many publications of the past decades (summarised e.g. in [4]), the notches cause stress concentrations in the timber beams. The stress concentrations can lead to an early, brittle failure of the timber beams, especially in regions of high shear forces. Therefore, the high shear forces occurring around the load

[1] Dominik Bissig, Institute of Structural Engineering, ETH Zurich, Switzerland, bissig@ibk.baug.ethz.ch
[2] Marcel Muster, Institute of Structural Engineering, ETH Zurich, Switzerland, muster@ibk.baug.ethz.ch
[3] Andrea Frangi, Institute of Structural Engineering, ETH Zurich, Switzerland, frangi@ibk.baug.ethz.ch

https://doi.org/10.52202/069179-0342

introduction of the point supported flat slabs can become the governing design parameter of the new hollow slab. A lower shear resistance of the hollow elements requires larger CLT elements introducing the loads into the point supports. The goal is to reduce the size of the CLT areas, to cut back on the usage of timber as much as possible. Therefore, a high shear resistance of the new hollow element is needed, and the optimisation of the grid intersection points is a crucial task in the current research project.

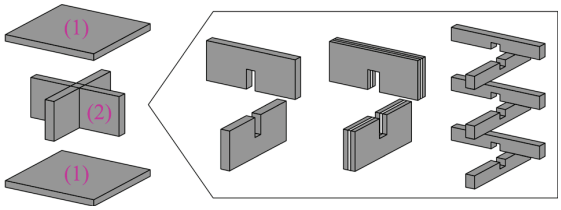

Figure 2: *Layout of the different compounds of the biaxial hollow slab elements and the different web intersection designs tested in* [5]. *(1) CLT plates, (2) GLT / CLT beams with the different notched intersection options.*

A first experimental investigation on biaxial hollow timber elements with different intersection types (as illustrated in Figure 2) was performed in 2021 at ETH Zurich [5]. The uniaxial 4-point bending tests were performed to find the bending stiffness, the shear stiffness and the shear resistance of the different element types. The experiments showed, that multiple smaller notches or the use of a wider CLT instead of a slimmer GLT beam grid increases the shear load bearing capacity of the element by 35% on average [5]. After the experiments, the three intersection types illustrated in Figure 2 were chosen to further investigate with finite element (FE) models.

To investigate the influence of the different geometrical properties on the different structural properties of the elements, the FE-models are parametrised, and a parameter study is performed. The main goal of the parameter study is to find an option with large shear resistance due to the reasons mentioned before. The bending resistance, bending stiffness and shear stiffness are also investigated, but are assumed to be less important. It is assumed that the bending resistance and the bending stiffness can easily be controlled with the hight of the element and the thickness of the CLT plates. According to previous experiences with the TS3 slab system, the shear stiffness has only a minor influence on the global deformations and vibrations in comparison to the bending stiffness. However, the influence of the notch geometry, the web width and web material on the shear resistance is of special interest for this investigation. It is assumed, that these are the most efficient parameters to be manipulated to enlarge the shear resistance. A literature review and the experimental campaign suggest that multiple smaller notches enlarge the shear resistance of all element geometries. Since the production of multiple small notches is more expensive than the production of one larger notch, the parameter study has to proof the structural benefits of the smaller notches over a variety of geometry combinations. Also, the influence of the web width on the shear resistance has to be investigated. A wider web (the same width is used in both directions) enlarges not only the webs cross sectional area, but also the width of the notch. The parameter study should also show, whether the use of CLT in the web is generally beneficial for the shear resistance. Finally, the findings from this parameter study are needed to further optimise and finalise the cross section geometry of the new slab elements.

2 MATERIAL AND METHODS

2.1 FRAMEWORK AND MODELLING

The parameter study was performed in the FE program Abaqus [6]. A Python script was used to generate and execute a volumetric, linear elastic model in Abaqus Standard. The script reads deformations and stresses from the output database generated by Abaqus and stores the information in text files. The text files were read and visualised with the help of a Matlab [7] script.

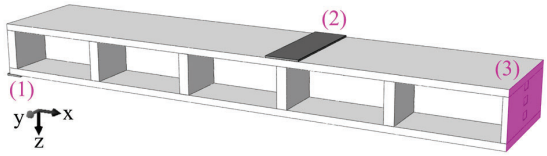

Figure 3: *Illustration of the FE model in Abaqus. (1) steel plate support, (2) steel plate load introduction, (3) symmetry plane.*

The 4-point bending test was modelled in Abaqus with volumetric timber elements. The timber plates were modelled as single parts and the timber webs were modelled as single parts with openings. To model CLT, the parts were partitioned, and each layer was assigned the correct material orientation. Side face gluing of all layers was assumed. The plate and web parts were connected rigidly with each other to form the assembly shown in Figure 3. A hard contact with a tangential friction coefficient of 0.3 was applied between timber and steel plates (support and load introduction), as well as between all timber parts that are not glued together. No glued connection was modelled at the notched intersection of the longitudinal and the cross web parts. The notches were modelled with 1 mm air around all three edges to account for the production. Each steel plate was constrained in all degrees of freedom to a reference point lying centrically below/above the plate (see Figure 4). The reference point at the support was fixed in the directions u_y, u_z (deflections), r_x and r_z (rotations), to model a rolling support. The reference point at the load introduction was fixed in u_x and u_y direction. A point load of $F_{cyl} = 10$ kN was introduced to the reference point above the load introduction steel plate. The symmetry plane in the middle of the specimen was fixed in the directions u_x, r_y, r_z.

The Abaqus mesh element type C3D8 (brick element with 8 integration points) was chosen. A preliminary investigation showed, that this element type has the best result quality to computation time ratio for the on hand study. The mesh size was chosen according to the CLT plate layer thickness h_h. For $h_h \leq 20$ mm, a mesh size of 20 mm was chosen, for $h_h > 20$ mm a mesh size of 30 mm was chosen. A mesh refinement region was

https://doi.org/10.52202/069179-0342

implemented around the notch nearest to the support and at the symmetry plane. In the refinement region, a mesh size of 10 mm was chosen. The refinement region stretched 60 mm from the cross web, followed by a mesh transition zone of 40 mm, as illustrated in Figure 4.

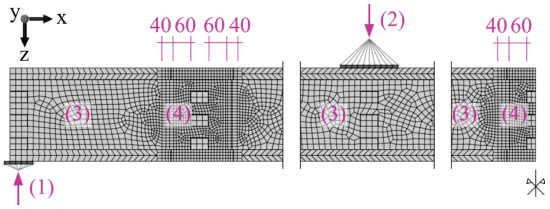

Figure 4: *Longitudinal section of a specimen in Abaqus with the mesh of C3D8 elements, generated according to the defined restrictions. (1) support on reference point, (2) load introduction to reference point, (3) general mesh 20..30 mm, (4) fine mesh 10 mm.*

The elastic material parameters for the longitudinal (L, 1), tangential (T, 2) and radial (R, 3) direction shown in Table 1 were used to model the timber parts. The material model does not distinguish between radial and tangential properties (transversely isotropic material model). Average values of the Poisson's ratio after [8] were used.

Table 1: *Elastic properties of the modelled timber parts for a moisture content of 12%.*

E_1 $E_2 = E_3$	11'500 MPa 300 MPa	Elastic modulus [9]
$G_{12} = G_{13}$ G_{23}	650 MPa 65 MPa	Shear modulus [9]
$\nu_{12} = \nu_{13}$ ν_{23}	0.395 0.41	Poisson's ratio [8]

To verify the FE-model with the experimental results, the actual average timber moisture content of 9% was taken into account. The moisture dependent stiffness parameters after Neuhaus [10] were used to scale the stiffness parameters listed in Table 1 according to Equation (1).

$$E_{FE} = E_{EN} \cdot \frac{E_{NH}(9\%)}{E_{NH}(12\%)} \quad (1)$$

with: E_{FE} Elastic modulus used in the FE-model
E_{EN} Elastic modulus defined in Table 1
E_{NH} Elastic modulus after [10] in dependence of the timber moisture content

2.2 GEOMETRY

The geometric properties of the modelled elements were parametrised to study their influence on the structural properties of the slab elements. The parameters illustrated in Figure 5 were varied with the values listed in Table 2.

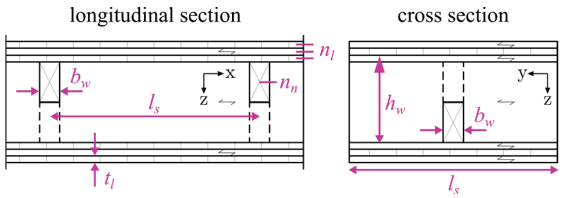

Figure 5: *Illustration of the geometric parameters that are varied within the scope of the parameter study (see Table 2). Longitudinal and cross section of one element configuration modelled with the setup of a uniaxial 4-point bending test.*

Table 2: *Parameters of the hollow elements that are varied within the scope of the parameter study (see Figure 5 for an illustration of the geometric parameters).*

Name	Range	Description
b_w	60, 120, 180 mm	web width
h_w	80, 180, 280 mm	web height
l_s	375, 500, 625 mm	web spacing
n_n	1, 3	number of notches
t_l	20, 40 mm	thickness of CLT layers
n_l	2, 3	number of CLT layers
PN	top, bottom	position of notch
GD	0°, 90°	grain dir. CLT top layer
MW	GLT, CLT	material web

The width of the element was chosen equal to the web spacing l_s to model a representative section of the slab. The number of openings between the cross web parts was kept at a constant number of $n_o = 5$. Thus, the total length of the specimen varied with the chosen web spacing l_s.
A total of 1728 combinations result from the parameters listed in Table 2. The following combinations were excluded from the analysis, since they are not viable either from a productional or from a structural point of view:

- $b_w = 180$ mm and $l_s = 375$ mm
- $h_w = 80$ mm and $n_n = 3$
- MW = CLT and $n_n = 3$

Thus, a total of 1024 geometry combinations result, which leads to the same number of models to be created.
Furthermore, six models with the geometric parameters given by the experimental analysis (see [5]) were created. These models were used to verify the FE results of the failure load and the stiffness by comparing them to the corresponding experimental results. The geometry and the naming of the verification models is summarised in Table 3 and described in detail in [5].

Table 3: *Names and geometry of the verification models. All verification models had a web hight* $\boldsymbol{h_w = 240}$ *mm, a web spacing* $\boldsymbol{l_s = 625}$ *mm, a CLT layer thickness* $\boldsymbol{t_l = 20}$ *mm and a number of CLT layers* $\boldsymbol{n_l = 2}$.

	NL-LX	NL-XL	NX-LX	NX-XL	CL-LX	LL-LX
	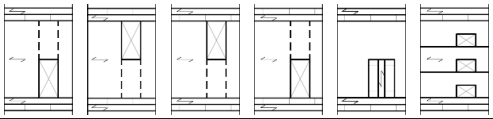					
b_w	60 mm	60 mm	60 mm	60 mm	80 mm	60 mm
n_n	1	1	1	1	1	3
PN	B	T	T	B	B	B

GD	0°	90°	0°	90°	0°	0°
MW	GLT	GLT	GLT	GLT	CLT	GLT

2.3 DATA OUTPUT AND CALCULATIONS

The deflections were evaluated in the pure bending region at the symmetry plane and at a distance of 250 mm from the load introduction point, as illustrated in Figure 6. The bending and shear stiffness can be calculated from the two deflections after Equation (2) and (6).

$$EI_{eff} = \frac{F_{cyl}\, a\, l_w^2}{8\,(w_2 - w_1)} \tag{2}$$

With the assumption that only bending deformations occur in the whole specimen, the apparent bending stiffness can be calculated from Equation (3).

$$EI_{app} = \frac{F_{cyl}}{24\, w_2}\,(3\, a\, l^2 - 4\, a^3) \tag{3}$$

Since the total deformation in the middle of the specimen compounds of bending and shear deformations, the shear stiffness GA_v can be calculated as follows.

$$w_2 = w_2(M) + w_2(V) \tag{4}$$

$$w_2 = \frac{F_{cyl}}{24\, EI_{eff}}(3\, a\, l^2 - 4\, a^3) + \frac{F_{cyl}\, a}{GA_v} \tag{5}$$

$$GA_v = \frac{F_{cyl}\, a}{w_2 - \frac{F_{cyl}}{24\, EI_{eff}}(3\, a\, l^2 - 4\, a^3)} \tag{6}$$

with:
- EI_{eff} Bending stiffness
- GA_v Shear stiffness
- EI_{app} Apparent bending stiffness, assuming $GA_v \to \infty$
- F_{cyl} Force applied per cylinder (10 kN)
- a Distance between support and load introduction (see Figure 6)
- l_w Distance between third point deformation measurements (see Figure 6)
- l Distance between supports (see Figure 6)
- w_i Deformation (see Figure 6)

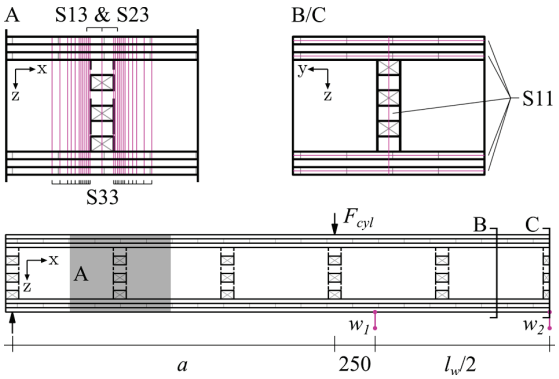

Figure 6: *Evaluation positions of the shear stress (S13, S23), stress perpendicular to grain (S33) and stress parallel to grain (S11) as well as the deformations w_i.*

The bending tension and compression stresses (S11) parallel to grain were evaluated in the pure bending region in the cross sections B and C illustrated in Figure 6. They were evaluated in the centre of each longitudinal layer of the plates and along a vertical section in the middle of the model. The shear (S13) and rolling shear (S23) stresses were evaluated along three vertical lines in the middle and 10 mm to the left and right of the notch next to the support as illustrated in Figure 6. The stresses perpendicular to grain (S33) were evaluated at the same notch, but along 12 vertical lines left and right of the notch. Since the self weight is neglected in the parameter study, the shear force between support and load introduction is constant. Hence, the shear stresses and the stresses perpendicular to grain were not measured at the support to avoid the local influence of the supporting steel plate. For the specimens with a GLT web, the vertical evaluation lines were placed in the centre of the web. To capture the stress perpendicular to grain in the specimens with a CLT web, the vertical evaluation lines in these models were placed in the layer with horizontal grain direction 1 mm from the edge of the web.

The evaluated maximum stresses were compared to the corresponding strength to estimate the load bearing capacity. Preliminary investigations showed that the peak stress positions of the different stress directions do not coincide. Thus, the load bearing capacity of each linear elastic model was estimated after Equation (7) and no stress interactions were considered.

$$F_R = \min\left\{F_{cyl} \cdot \frac{f_i}{\sigma_i}\right\} \tag{7}$$

with:
- F_R Load bearing capacity
- F_{cyl} Applied cylinder force
- f_i Strength in direction *i*
- σ_i Maximum stress occurring in direction *i*

To estimate the load bearing capacity, the average strength values for GL24h listed in Table 4 were used. The compression strength perpendicular to grain was neglected since the tension strength perpendicular to grain is decisive in every case due to symmetry. The tensile strength perpendicular to grain was chosen after the glulam specimens tested by [11] for a small reference volume of 0.75 to 1.5 dm^3.

Table 4: *Mean strength values for GL24h used to estimate the load bearing capacity.*

Name		Value (MPa)	Source
S11	$f_{t,0,m}$	27	[12]
	$f_{c,0,m}$	40	[12]
S13	$f_{v,m}$	4.1	[13]
S23	$f_{r,m}$	1.88	[14]
S33	$f_{t,90,m}$	1.5	after [11]

2.4 EVALUATION METHODS

The stress and strain output database of the verification FE-models was analysed manually in Abaqus' 3D viewer and compared to the automatically produced result data vectors to ensure the quality of the automated data output.

https://doi.org/10.52202/069179-0342

Due to the number of models used in the parameter study, only the automated data output was used for its analysis. The Kendall rank correlation coefficient [15] was used to get an overview of the relations between the different geometry parameters and the structural properties. Furthermore, box- and scatter plots were used to validate the correlation numbers visually and to get a quantitative overview of the results. The boxplots show a box between the 25th and the 75th percentile. All values lying outside the boundaries of 1.5 times the interquartile range are marked as outliers. The median is marked by the centre line and the notches indicate the 5% significance range of the median after [16].

3 RESULTS AND DISCUSSION

3.1 VERIFICATION

Figure 7 shows the force displacement diagrams from the experiments and from the corresponding linear elastic FE models. A longitudinal section and the short name in each diagram indicate the corresponding specimen type. The first two failures estimated by the FE model are indicated in the diagrams with circles.

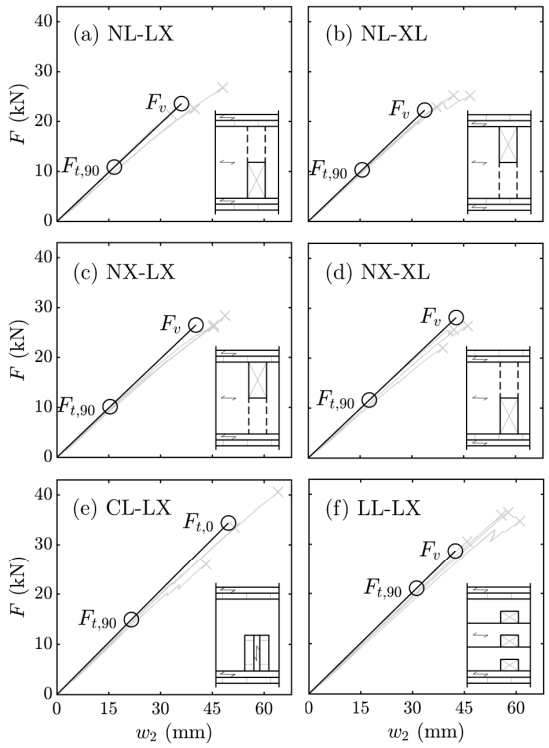

Figure 7: *Force displacement diagrams of the verification models. Results from the FE analysis (black) and the experimental analysis (grey). The circles indicate the first two failures estimated by the FE model.*

Only a negligibly small difference between the grey lines and the black line can be seen between 10% and 40% of the estimated failure load. This indicates that the model predicts the stiffness well in the region of interest. Towards the end of the curve, the grey lines show larger deflections than the black line. This softening is probably caused by the cracks propagating from the notch's corners along the web, which is not reproduced by the linear elastic FE-models. Since the softening occurs in a late state of the experiment, it is not relevant for the derivation of the stiffness parameters and the chosen method is assumed to be suitable. The estimation of the failure load is less straight forward. As observed in the experimental campaign, the first failure occurs in tension perpendicular to grain ($F_{t,90}$) for all specimen types. The magnitude of the first failure load also corresponds well with the observations made during the experiments. It was observed that the cracks formed at the notches corners and expanded until a shear failure occurred. The shear failure (F_v) is also predicted as a second failure by the FE model for the types NL, NX and LL. Although the cross section reduction by crack propagation is not taken into account by the FE model, the magnitude of the shear failure load for these types fits the observed failure load well. The second failure load of the CL type is predicted to be in tension parallel to grain ($F_{t,0}$) in the bending region. No bending failure was observed in the experimental campaign, however, a shear and rolling shear failure in the glue line was observed after the crack propagation. Nevertheless, the first failure type is predicted well for all specimen types. Thus, the first failure type is chosen for further comparisons of the shear resistance. Although this failure does not necessarily correspond to a global failure of the specimen, it still allows for a relative comparison of the models analysed in the parameter study.

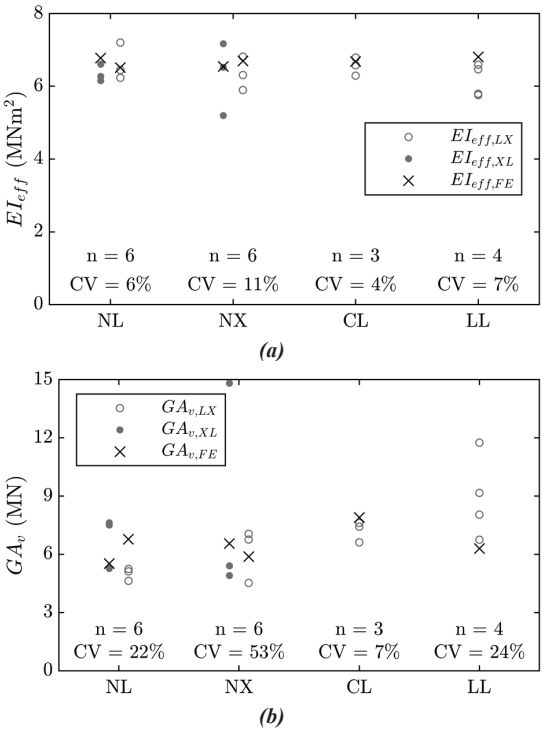

Figure 8: *Bending stiffness* ***(a)*** *and shear stiffness* ***(b)*** *of the different element types, derived from the experimental campaign and the FE-models.*

Figure 8 compares the experimentally determined and numerically predicted bending (EI_{eff}) and shear stiffness

(GA_v). The experimentally determined shear stiffness shows a large scattering for the element type LL. This can partly be explained by the fact, that for two of the LL specimens, only one of two LVDTs measuring w_1 was used due to a malfunction of the other one. The outlier shear stiffness measurement of the specimen type NL showed a large longitudinal crack in the web in the pure bending region already before the test. It is assumed that the specimen cracked due to swelling and shrinking and that the larger deformations in the pure bending region lead to an underestimation of the bending stiffness and an overestimation of the shear stiffness. Given the small number of experiments and the scattering of the results, it still can be stated that the FE-model predicts both stiffnesses accurately for all specimen types. Thus, the chosen material parameters, the element type and the mesh size are assumed to be suitable.

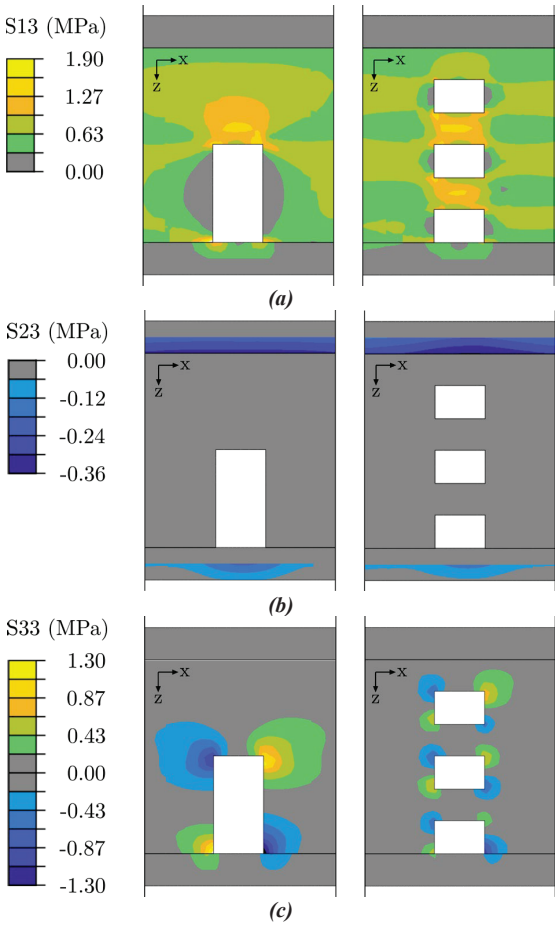

Figure 9: *Stresses acting near the first notch after the support of the specimens NL-LX (left) and LL-LX (right). Acting on the sections: shear load V = 10 kN, bending moment M = 6.3 kNm.* ***(a)*** *shear stress (S13 =* $\boldsymbol{\sigma_v}$*),* ***(b)*** *rolling shear stress (S23 =* $\boldsymbol{\sigma_r}$*),* ***(c)*** *stress perpendicular to the grain (S33 =* $\boldsymbol{\sigma_{t/c,90}}$*).*

Figure 9 illustrates the shear and rolling shear stress as well as the stress perpendicular to grain in the NL-LX and the LL-LX models at the notch next to the support (section A as illustrated in Figure 6). Figure 9 (a) and (b) show, that the largest shear and rolling shear stresses occur in the centre line of the notches. The magnitude and the volume subjected to large shear stresses is similar for both the NL and the LL model. Figure 9 (c) shows, that the NL specimen experiences a higher peak in stresses perpendicular to grain than the LL specimen. Additionally, the timber volume subjected to stresses perpendicular to grain is larger for the NL specimen. Figure 10 illustrates the bending stress of the NL-LX and the LL-LX models at the symmetry plane. It shows, that the tension stress parallel to grain is largest near the web and a stress peak forms under the notch. This peak is higher for the NL model than for the LL model. Nevertheless, the full width of the flange is activated in tension and compression in both models.

It can be concluded that the chosen positions for the evaluation of the stresses as illustrated in Figure 6 cover the maximum stress peaks for all stress directions. This can also be shown for the other reference specimens NX and CL.

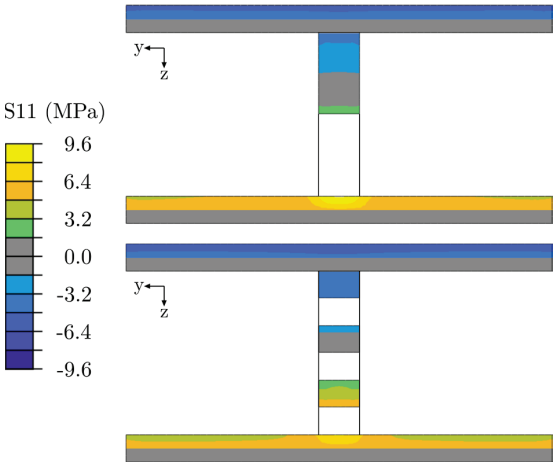

Figure 10: *Bending stress (S11 =* $\boldsymbol{\sigma_{t/c,0}}$*, resp.* $\boldsymbol{\sigma_m}$*) at the symmetry plane of the specimens NL-LX (top) and LL-LX (bottom). Acting on the sections: bending moment M = 18.75 kNm.*

3.2 PARAMETER STUDY

The Kendall rank correlation coefficient for the different geometry parameters and the different structural properties of the elements is shown in Figure 11. This coefficient can only be used to get a first overview of the results, since the coefficient was calculated over the whole dataset and some geometry combinations were excluded from the analysis from the beginning (see Section 2.2). The presented results were normalised for one meter width.

The absolute value of all correlations over the whole dataset is smaller than 0.6, which can be explained by the fact, that all structural parameters are influenced by multiple geometry parameters. Nevertheless, the figure shows, which geometrical parameters can be tackled to manipulate the different structural parameters efficiently. As expected, the bending resistance and the bending stiffness show the largest positive correlation with the height of the web and the thickness of the CLT plates

https://doi.org/10.52202/069179-0342

defined by the number (n_l) and thickness (t_l) of the single CLT layers. They also show a small negative correlation with the grain direction, which can be explained by the modelling of three-layered plates, which are stronger in one direction. Both parameters show little to no correlation with the web width and the web spacing. Since the bending resistance and the bending stiffness can easily be manipulated with the geometry parameters mentioned and since they are not decisive for the success of the hollow slab system, they are not discussed further.

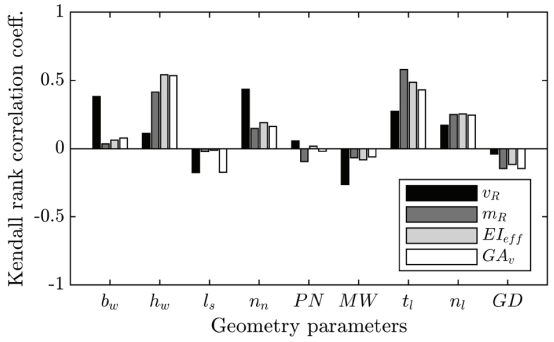

Figure 11: *Kendall rank correlation coefficient for the geometry parameters explained in Table 2 (positive correlation with respect to the values listed in Table 2 from left to right) and the structural parameters* $\boldsymbol{v_R}$ *(shear resistance),* $\boldsymbol{m_R}$ *(bending resistance),* $\boldsymbol{EI_{eff}}$ *(bending stiffness) and* $\boldsymbol{GA_v}$ *(shear stiffness). All structural parameters are evaluated per meter width.*

The shear stiffness also shows the largest positive correlation with the hight of the web and the thickness of the CLT plates, which have a direct influence on the cross-sectional area. It is assumed that the web width shows only a small positive correlation with the shear stiffness due to the exclusion of the mentioned parameter combination of a web width of 180 mm and a web spacing of 375 mm. The web spacing and the shear stiffness show a small negative correlation, which implies that a smaller web spacing is beneficial for the shear stiffness. Since the shear stiffness has only a minor impact on the global deformations of the hollow timber slab, it is not discussed further.

The position of the notch shows little to no correlation with any of the structural parameters. The negligible influence of the position of the notch can also be shown with more detailed scatter- and box plots and the findings coincide with the experimental investigations. The grain direction shows no correlation with the shear resistance and it shows only a small negative correlation with the other structural parameters. Therefore, these parameters are not discussed further.

The shear resistance is mainly influenced by the web width and the number of notches. The width of the web shows a positive correlation with the shear resistance. Thus, the positive effect of a wider web seems to dominate the assumed negative influence of a wider notch (see also Figure 12). The hight of the web does not correlate with the shear resistance, which is an indicator that the shear resistance is dominated by a failure in tension perpendicular to grain. A closer examination shows, that all 1024 models first fail in tension perpendicular to grain. The web spacing and the shear resistance show a small negative correlation, which implies that a smaller web spacing is beneficial for the shear resistance. It is assumed that this correlation would even be larger, if the combination with a web width of 180 mm and a web spacing of 375 mm would not have been excluded from the analysis. As assumed, the number of notches correlates positively with the shear resistance (see Figure 12). The thickness and number of the CLT plate layers also show a positive, but smaller correlation with the shear resistance. Since the plate thickness should stay as small as possible to save as much timber as possible, these parameters are not predestined to enlarge the elements shear resistance. The influence of web width, web spacing, number of notches and thickness of CLT plate layers on the shear resistance is illustrated in Figure 12. The figure confirms the previously stated assumptions and findings.

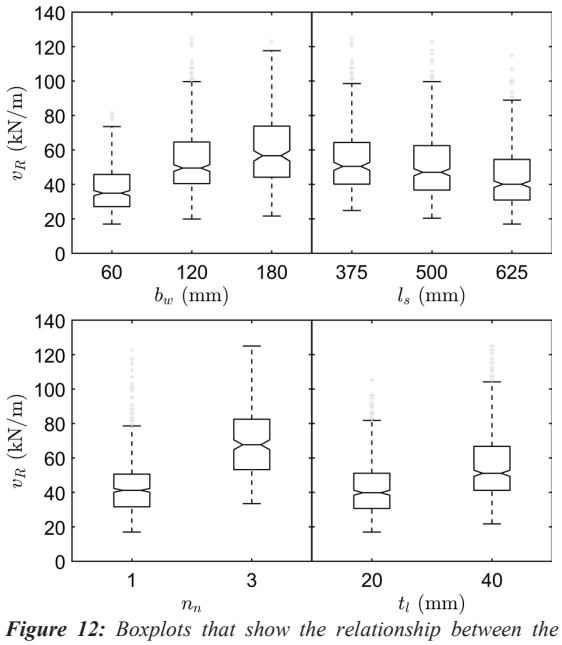

Figure 12: *Boxplots that show the relationship between the shear resistance and the web width (*$\boldsymbol{b_w}$*), the web spacing (*$\boldsymbol{l_s}$*), the number of notches (*$\boldsymbol{n_n}$*) and the thickness of the CLT plate layers (*$\boldsymbol{t_l}$*) for all models analysed within the parameter study.*

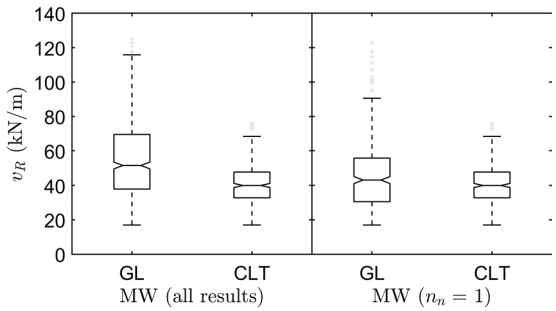

Figure 13: *Boxplots that illustrate the influence of the different web materials (MW) on the shear resistance. Two datasets are illustrated: all results (left) and only specimens with one notch (right).*

The material of the web shows a negative correlation with the shear resistance, which implies that using CLT to build the web does not bring benefits. As illustrated in Figure 13, the effect of a CLT web disappears in the statistical evaluation due to other, more important geometry parameters. The height of the notch dominates the influence on the shear resistance and the negative correlation partially originates from the fact, that the combinations with CLT web and three notches were excluded from the analysis. Figure 13 illustrates the relationship between the shear resistance and the material of the web for two different sets of results. If all results are considered, a negative correlation and a significantly smaller median follows for the CLT web specimens. If only the results for specimens with one notch ($n_n = 1$) are plotted, no significant difference between the medians can be found. Additionally, a smaller scattering of the CLT web specimens can be observed. This may arise from the measuring method of the stresses perpendicular to grain. It is possible that the stress measured only 1 mm from the edge of the CLT web captured a numerical stress peak and thus leads to more conservative shear resistance estimations. But even if the CLT web specimens showed a slightly higher shear resistance, they should not be preferred over the glulam option with one notch, since the stress concentration between web and plate will be the same for both options. The reinforcing vertical middle CLT layer can only be activated in the centre of the web, not at the boundary between plate and web.

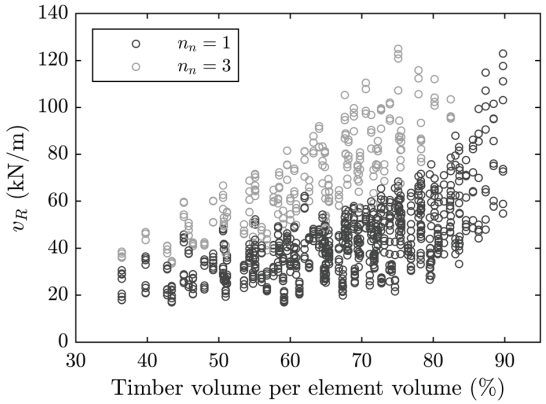

Figure 14: *Shear resistance of all geometry combinations plotted over their average timber volume per element volume. The number of notches ($\boldsymbol{n_n}$) of the individual specimens is illustrated by the marker's brightness.*

The correlations indicate that the shear resistance of the biaxial hollow slab elements is most efficiently maximised by using multiple notches, a wider web and a smaller web spacing. Figure 14 shows a plot of the shear resistance of each geometry combination over its average timber volume per element volume. The two groups of elements with only one notch and elements with three notches represented in black and grey can easily be distinguished. It can be seen, that the elements with three notches have a larger shear resistance overall. The plot clearly illustrates that multiple notches outrival the single notched web specimens in terms of shear resistance over the whole range of geometry combinations. It also shows that the largest shear resistances are achieved by using 70% of timber per element volume or more. As described in Section 1, the timber volume of the hollow elements should be as small as possible, and it should not exceed 70% of the total volume of the element. Thus, a geometry with multiple notches should be chosen in favour of an option with only one notch to build a biaxial hollow slab system.

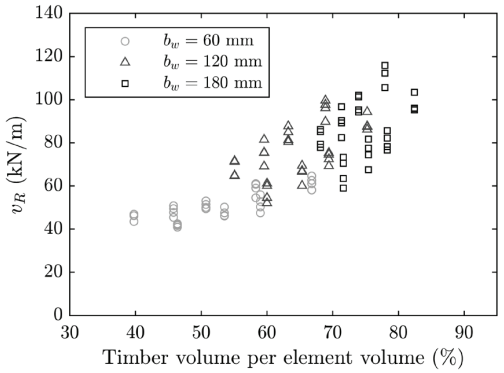

Figure 15: *Shear resistance of the specimens with three notches ($\boldsymbol{n_n = 3}$) and a web spacing ($\boldsymbol{l_s}$) of 500 mm. The web width ($\boldsymbol{b_w}$) of the individual specimens is illustrated by the markers shape and brightness.*

Enlarging the web width also leads to higher shear resistances, as illustrated in Figure 15 for specimens with three notches ($n_n = 3$) and a web spacing (l_s) of 500 mm. The overall smallest shear resistance is achieved with a web width of 60 mm, whereas the overall largest shear resistance is achieved with a web width of 180 mm. The figure also illustrates that less timber can be saved with wider webs. Since the timber volume of the hollow elements should be as small as possible, the results suggest, that web widths larger than 120 mm are not efficient.

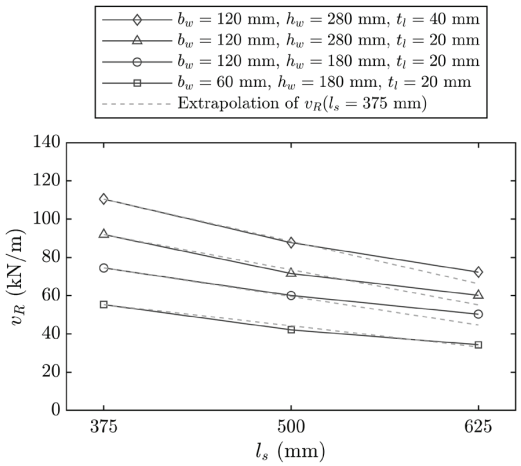

Figure 16: *Shear resistance over web spacing for four example geometry combinations with the common parameters $\boldsymbol{n_n = 3}$, $\boldsymbol{n_l = 2}$, $\boldsymbol{PN = bottom}$, $\boldsymbol{GD = 0°}$, $\boldsymbol{MW = GLT}$ and the varied parameters listed in the legend. The dashed line shows the shear resistance estimated by linear extrapolation of the shear resistance per web with $\boldsymbol{l_s = 375}$ mm.*

https://doi.org/10.52202/069179-0342

Figure 16 illustrates, how the web spacing influences the shear resistance on four different geometry combinations on which only the web spacing was varied. The shear resistance varies linearly with the web spacing. The dashed line in the graph was calculated with the shear resistance per web of the specimens with $l_s = 375$ mm. This shear resistance was linearly extrapolated to get the shear resistance per meter width for web spacings of 375 mm, 500 mm, and 625 mm. The results only marginally deviate from the dashed lines. Thus, it is assumed that the shear resistance varies directly proportional with the web spacing for values within the analysed boundaries and no mentionable stress interactions resulting from smaller web spacings occur.

4 CONCLUSIONS AND OUTLOOK

As expected, the bending resistance and the bending stiffness of the hollow elements can easily be enlarged by enlarging the thickness of the CLT plates and the total thickness of the elements. The same parameters have a positive influence on the shear stiffness too, which is however, less important than the bending stiffness for the serviceability limit state design. Multiple notches, a wider web and a closer web spacing have a positive influence on the shear resistance of the elements. The shear resistance of elements with multiple notches is significantly larger than the one of elements with one single notch over the whole set of geometry combinations. The number of notches proves to be the parameter with the largest influence on the shear resistance of the elements. Web widths larger than 120 mm lead to larger shear resistances, but also consume more timber and are consequently not to be used. The shear resistance per meter width of the element is directly proportional to the web spacing. In opposition to the initial assumption, no positive influence of a CLT web was found.

The different geometry combinations have been compared to each other and the relative best solutions and methods to optimise the mechanical properties were found. To find the absolute best solution for different point supported slab layouts, further studies are needed. Only by comparing different slab layouts, the total timber saving and the impact of the production cost on the total slab cost can be estimated. Hence, different examples of point supported slab arrangements should be analysed. Furthermore, a suitable analytical calculation method is of great importance to allow for an easy and efficient design process. Different analytical models for the calculation of bending and shear resistance and stiffness will be analysed and compared to the data achieved with the FE parameter study.

ACKNOWLEDGEMENT

The presented research project is funded by Innosuisse and supported by the project partners Timber Structures 3.0 AG, Schilliger Holz AG and Henkel & Cie AG. The research project is a collaboration between the ETH Zurich and the Bern University of Applied Sciences.

REFERENCES

[1] S. Zöllig, M. Muster, and A. Themessl, “Butt-Joint Bonding of Timber as a Key Technology for Point-Supported, Biaxial Load Bearing Flat Slabs Made of Cross-Laminated Timber,” *IOP Conf. Ser. Earth Environ. Sci.*, vol. 323, p. 012144, 2019.

[2] Timber Structures 3.0 AG, “References,” 2022. [Online]. https://www.ts3.biz/en/referenzprojekte/. [Accessed: 21-Feb-2023].

[3] S. Franke, B. Franke, and F. J. Niederwolfsgruber, “Bi-Axial Load Transfering Timber Grid-Box Elements for Floor Systems,” in *Proceedings of the 2021 World Conference on Timber Engineering (WCTE)*, 2021.

[4] R. Jockwer, R. Steiger, and A. Frangi, “State-of-the-Art Review of Approaches for the Design of Timber Beams with Notches,” *J. Struct. Eng.*, vol. 140, no. 3, p. 04013068, 2014.

[5] D. Bissig and A. Frangi, “Variantenstudium zur Entwicklung einer zweiachsig tragenden Hohlkastendecke aus Holz,” in *9. Doktorandenkolloquium „Holzbau Forschung + Praxis“ (DoKo 2022), Stuttgart*, 2022, pp. 89–96.

[6] Dassault Systèmes, “Abaqus 2019.” 78946 Vélizy-Villacoublay Cedex (FR), 2019.

[7] MathWorks, “Matlab R2021b.” Natick, Massachusetts 01760-2098 (US), 2021.

[8] J. Bodig and B. Jayne, *Mechanics of wood and wood composites*. Florida: Krieger Publishing Company, 1993.

[9] CEN, “SN EN 14080:2013 Holzbauwerke – Brettschichtholz und Balkenschichtholz – Anforderungen,” vol. 2. Schweizer Ingenieur- und Architektenverein, 2013.

[10] H. Neuhaus, “Elastizitätszahlen von Fichtenholz in Abhängigkeit von der Holzfeuchtigkeit,” Bochum, 1981.

[11] H. J. Blaß and M. Schmid, “Ermittlung der Querzugfestigkeit von Voll- und Brettschichtholz,” Karlsruhe, 1998.

[12] M. Frese, “Computergestützte Verfahren zur pragmatischen Beurteilung der Tragwiderstände von Brettschichtholz: Zusammenfassung exemplarischer Simulationsstudien,” Karlsruher Institut für Technologie, 2016.

[13] G. Schickhofer, “Determination of shear strength values for GLT using visual and machine graded spruce laminations,” in *CIB-W18 Meeting 34*, 2001, no. 34-12–6.

[14] T. Ehrhart, R. Brandner, G. Schickhofer, and A. Frangi, “Rolling Shear Properties of some European Timber Species with Focus on Cross Laminated Timber (CLT): Test Configuration and Parameter Study,” in *INTER Meeting 48*, 2015, no. 48-6–1.

[15] M. G. Kendall, *Rank correlation methods*, 4th ed. London: Griffin, 1970.

[16] R. McGill, J. W. Tukey, and W. A. Larsen, “Variations of box plots,” *Am. Stat.*, vol. 32, no. 1, pp. 12–16, 1978.